# Complex Images for Electrostatic Field Computation in Multilayered Media

Y. Leonard Chow, *Member, IEEE*, Jian Jun Yang, *Member, IEEE*, and Gregory E. Howard

*Abstract*—**A rapidly convergent algorithm is presented to find the spatial simulated images of a point charge in multilayered media. The simulated images turn out to be complex; i.e., they have complex amplitudes and are located at complex positions. Surprisingly, these complex images give very accurately (error ~ 0.1%) the static field in multilayered media. The examples of two- and three-layered media are examined, together with the available exact image solutions of singly or doubly infinite series. It is believed that the accuracy and rapid convergence of the complex images derive from the extra degrees of freedom arising from the imaginary components of the amplitude and position.**

## I. Introduction

THE Green's function–moment method technique has been used for the static analysis of 2-D transmission lines [1], [2] and 3-D interdigital capacitors [3]. For a two-layered dielectric with or without a ground plane, the Green's function is represented as an infinite series obtained from image theory [1], [3]. For the three-layered media, the Green's function is represented as a doubly infinite series of images [2]. As pointed out in [4], the extension of this type of Green's function to more than three dielectric layers is impractical, because for $N$ dielectric layers, it should consist of an $N-1$ multiply infinite series.

In this paper, we present an approach which makes it practical to find the simulated images of a point charge in multilayered media. For two-layered or three-layered media, instead of an infinite or a doubly infinite series of images, the Green's function presented in this paper consists of only four terms, i.e., an effective source term plus three complex images. This new Green's function is shown to give an error of the order of 0.1% when compared with the rigorous infinite series solution. Also, the Green's function for the layered media with more than four layers still consists of four similar terms.

Complex image theory has been successfully used to solve the dynamic radiation problem in layered media [6]–[9]. For static field computations in layered media, it is shown in this paper that the *complex* images can also give the *real* field. To find the complex images, the same numerical algorithm, Prony's method [11], can be used. No matter how many layers are involved, the sample points used in Prony's method are obtained in the same manner. This situation is analogous to using optimized simulated images [10] for the field of a point charge outside of an arbitrarily shaped conductor.

In the following presentation of the theory, we take two- and three-layered media as examples where the exact image solutions of infinite series are available. They allow a comparison between the complex image solution and the exact image solution. After this comparison, a general procedure is presented to find the complex images of a point charge in multilayered media.

Manuscript received November 13, 1990; revised February 25, 1991. This work was supported by the Communications Research Center, Canada, under Contract 36001-9-3581/01-SS.

The authors are with the Department of Electrical and Computer Engineering, University of Waterloo, Waterloo, Ontario, Canada N2L 3G1.

IEEE Log Number 9100147.

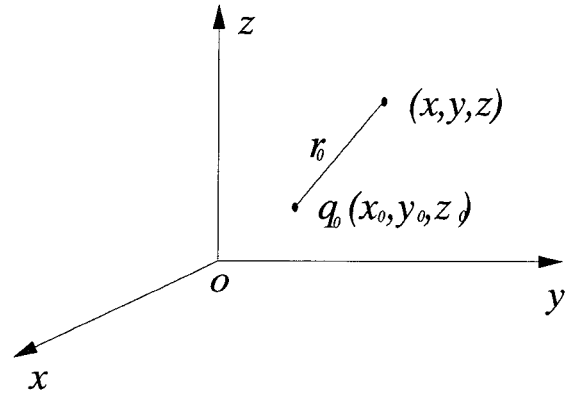


Fig. 1. Point charge in free space.

## II. Theory

### A. Point Charge in Free Space

For easy understanding and comparison with the multilayered cases, we begin with a point charge $q_0$ in free space, as shown in Fig. 1. The spatial potential function of this point charge is known from Coulomb's law:

$$\Phi = \frac{q_0}{4\pi\epsilon_0 r_0} \tag{1}$$

where

$$r_0 = \sqrt{(x-x_0)^2+(y-y_0)^2+(z-z_0)^2}. \tag{2}$$

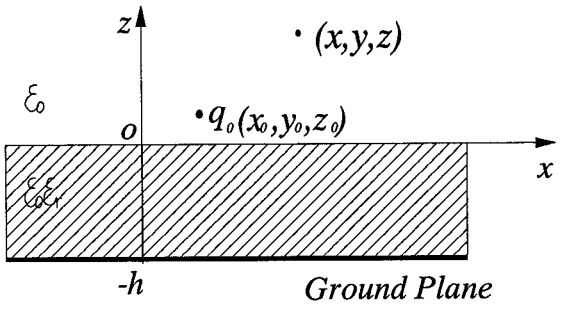


Fig. 2. Point charge on a microstrip substrate.

Through the Fourier transform, it is easily shown that the spectral potential function is

$$\tilde{\Phi}(\gamma, z, z_0) = \frac{q_0}{2\epsilon_0 \gamma} e^{-\gamma|z-z_0|} \tag{3}$$

where

$$\gamma = \sqrt{k_x^2 + k_y^2}. \tag{4}$$

The spatial potential function (1) is the inverse Fourier transformation of the spectral potential function (3), i.e.,

$$\frac{q_0}{4\pi\epsilon_0 r_0} = \left(\frac{1}{2\pi}\right)^2 \int\int_{-\infty}^{+\infty} \frac{q_0}{2\epsilon_0\gamma} \cdot e^{-\gamma|z-z_0|} e^{-jk_x(x-x_0)} e^{-jk_y(y-y_0)}\, dk_x\, dk_y. \tag{5}$$

It can be easily shown by direct substitution that the spatial potential function (1) satisfies the Possion equation even if the source location $(x_0, y_0, z_0)$ is complex. The same applies to (5), which is the identity used below.

### *B. Point Charge on a Microstrip Substrate*

As shown in Fig. 2, a point charge $q_0$ is located at $(x_0, y_0, z_0)$ above a microstrip substrate. The spectral domain potential function $\tilde{\Phi}$ at $(x, y, z)$, which satisfies the Possion equation and all the boundary conditions, can be easily derived using the transmission line theory given in [5]:

$$\tilde{\Phi} = \frac{q_0}{2\epsilon_0\gamma} \cdot \left( e^{-\gamma|z-z_0|} + \frac{K - e^{-2\gamma h}}{1 - Ke^{-2\gamma h}} e^{-\gamma(z+z_0)} \right), \quad z \geqslant 0, \quad z_0 \geqslant 0 \tag{6}$$

where $K = (1-\epsilon_r)/(1+\epsilon_r)$. Expanding (6) into a Taylor series:

$$\tilde{\Phi} = \frac{q_0}{2\epsilon_0\gamma} \left( e^{-\gamma|z-z_0|} + Ke^{-\gamma(z+z_0)} + \sum_{n=1}^{\infty} K^{n-1}(K^2-1) e^{-\gamma(z+z_0+2nh)} \right) \tag{7}$$

and substituting (7) into the identity (5), we have

$$\Phi = \frac{q_0}{4\pi\epsilon_0} \left( \frac{1}{r_0} + \frac{K}{r_0'} + \sum_{n=1}^{\infty} K^{n-1}(K^2-1) \frac{1}{r_n} \right) \tag{8}$$

where

$$r_0 = \sqrt{(x-x_0)^2 + (y-y_0)^2 + (z-z_0)^2}$$

$$r_0' = \sqrt{(x-x_0)^2 + (y-y_0)^2 + (z+z_0)^2}$$

$$r_n = \sqrt{(x-x_0)^2 + (y-y_0)^2 + (z+z_0+2nh)^2}.$$

Expression (8) stands for an exact image solution for the microstrip problem in three dimensions, which is equivalent to that in two dimensions given by Silvester [1]. This exact image solution will be taken as the benchmark of the complex image solution discussed below.

To get the complex image solution, the following two steps are always taken:

1) Find the limit of $\gamma \to \infty$ of the function in (6), i.e.,

$$\lim_{\gamma\to\infty} \frac{K - e^{-2\gamma h}}{1 - K^{-2\gamma h}} = K. \tag{9}$$

2) Subtract the above limit from the original function and match the remainder with a short sum of decaying exponential functions, i.e.,

$$\frac{K - e^{-2\gamma h}}{1 - Ke^{-2\gamma h}} - K \doteq \sum_{i=1}^{N} a_i e^{b_i \gamma} \tag{10}$$

where $a_i$ and $b_i$ are the complex coefficients determined through Prony's method [11]. $N$ is the number of exponential terms, generally taken as $2 \sim 5$. In this paper, $N = 3$.

Substituting (10) into (6), and taking the inverse Fourier transformation of $\tilde{\Phi}$, we have

$$\Phi \doteq \frac{q_0}{4\pi\epsilon_0} \left( \frac{1}{r_0} + \frac{K}{r_0'} + \sum_{i=1}^{N} \frac{a_i}{r_i} \right) \tag{11}$$

where $r_i = \sqrt{(x-x_0)^2 + (y-y_0)^2 + (z+z_0-b_i)^2}$ is a complex distance, with $b_i$ being complex.

In (11), if $z = z_0 = 0$, then the first two terms $(1/r_0 + K/r_0')$ can be written as

$$\frac{2}{(1+\epsilon_r)} \cdot \frac{1}{r_0}$$

which is essentially an *effective* homogeneous medium potential function wherein the dielectric constant is equal to the average of two media. The short series can be considered as a correction to the effective homogeneous medium term, each standing for a simulated image with complex amplitude $a_i$ located at complex location $(x_0, y_0, z_0 - b_i)$.

Table I lists the complex image coefficients for two microstrip substrate examples. It is seen that the complex image coefficients are either *paired as complex conjugate of each other*, or just *singles and real*. This explains why the complex images give a real-valued field. Table II lists the values of the function $\Phi$ computed by the exact image solution (8) and the complex image solution (11). It is seen that the difference between these two solutions is of the order of 0.1% for all the source-to-field point distances tabulated.

TABLE I
COMPLEX IMAGES OF A POINT CHARGE ON A MICROSTRIP SUBSTRATE

| | $\epsilon_r = 2.55$, $h = 1.0$ mm | | $\epsilon_r = 9.6$, $h = 1.0$ mm | |
|---|---|---|---|---|
| $i$ | $a_i$ | $b_i$ ($\times 10$ mm) | $a_i$ | $b_i$ ($\times 10$ mm) |
| 1 | $-0.7802$ | $-0.1985$ | $-0.2725$ | $-0.1912$ |
| 2 | $0.1084 + j0.3897$E-1 | $-0.3886 + j0.1009$ | $0.4367$E-1 $+ j0.1255$E-1 | $-0.3197 + j0.1474$ |
| 3 | $0.1084 - j0.3897$E-1 | $-0.3886 - j0.1009$ | $0.4367$E-1 $- j0.1255$E-1 | $-0.3197 - j0.1474$ |

TABLE II
POTENTIAL FUNCTION $\Phi$ COMPUTED BY THE EXACT IMAGE SOLUTION AND THE COMPLEX IMAGE SOLUTION $\left(z_0 = 0,\ z = 0,\ \rho = \sqrt{(x - x_0)^2 + (y - y_0)^2}\right)$

| | $\epsilon_r = 2.55$, $h = 1.0$ mm | | $\epsilon_r = 9.6$, $h = 1.0$ mm | |
|---|---|---|---|---|
| $\rho$ (mm) | Exact Image Solution (8) | Complex Image Solution (11) | Exact Image Solution (8) | Complex Image Solution (11) |
| 0.1 | 5298.49 | 5298.45 | 1729.14 | 1729.03 |
| 0.6 | 619.37 | 619.36 | 192.20 | 192.16 |
| 1.1 | 223.66 | 223.67 | 64.25 | 64.27 |
| 1.6 | 99.41 | 99.43 | 25.69 | 25.72 |
| 2.1 | 49.17 | 49.17 | 11.14 | 11.14 |
| 3.1 | 15.13 | 15.13 | 2.49 | 2.48 |

### C. Point Charge in a Substrate–Superstrate Structure

As shown in Fig. 3, a point charge $q_0$ is located at the interface of two media (i.e., $(z_0 = 0)$). The spectral domain potential function $\tilde{\Phi}$ at the interface of the two media (i.e., $(z = 0)$) is derived using the transmission line theory given in [5]:

$$\tilde{\Phi} = \frac{q_0}{2\epsilon_0 \epsilon_{r1} \gamma} \cdot A(\gamma)$$

$$A(\gamma) = \frac{2}{(\epsilon_{r1} + cth\gamma h_1)/(1 + \epsilon_{r1} cth\gamma h_1) + (\epsilon_{r2}/\epsilon_{r1}) cth\gamma h_2}. \tag{12}$$

Following the same two steps as those in subsection II-B, we have

$$\lim_{\gamma \to \infty} A(\gamma) = \frac{2}{1 + \epsilon_{r2}/\epsilon_{r1}} \tag{13}$$

$$A(\gamma) - \frac{2}{1 + \epsilon_{r2}/\epsilon_{r1}} \doteq \sum_{i=1}^{N} a_i e^{b_i \gamma}. \tag{14}$$

Substituting (14) into (12), and taking the inverse Fourier transformation of $\tilde{\Phi}$, we have

$$\Phi \doteq \frac{q_0}{4\pi\epsilon_0 \epsilon_{r1}} \left( \frac{2}{1 + \epsilon_{r2}/\epsilon_{r1}} \frac{1}{r_0} + \sum_{i=1}^{N} \frac{a_i}{r_i} \right). \tag{15}$$

The first term in (15) can again be considered an *effective* homogeneous medium potential function with dielectric constant equal to the average of two media. The short series is, again, a correction to the effective homogeneous medium term.

For comparison, following the stated procedure of [2], the exact image solution of the substrate–superstrate in Fig. 3 is derived in terms of a doubly infinite series:

$$\Phi = \frac{q_0}{4\pi\epsilon_0} \cdot \frac{1}{\epsilon_{r1} + \epsilon_{r2}} \cdot \sum_{n=0}^{\infty} \sum_{(n_1, n_2, n_3 = 0)}^{n} \frac{n!}{n_1! n_2! n_3!} (-1)^{n_3} K_1^{n_1 + n_3} K_2^{n_2 + n_3} \cdot \left( \frac{1}{r_{n1}} - \frac{K_1}{r_{n2}} - \frac{1}{r_{n3}} + \frac{K_1}{r_{n4}} \right) \tag{16}$$

where

$$n_1 + n_2 + n_3 = n \qquad K_1 = (1 - \epsilon_{r1})/(1 + \epsilon_{r1}) \qquad K_2 = (\epsilon_{r1} - \epsilon_{r2})/(\epsilon_{r1} + \epsilon_{r2})$$

$$r_{n1} = \sqrt{(x - x_0)^2 + (y - y_0)^2 + [2n_1(h_1 + h_2) + 2n_2 h_2 + 2n_3 h_1]^2}$$

$$r_{n2} = \sqrt{(x - x_0)^2 + (y - y_0)^2 + [2n_1(h_1 + h_2) + 2n_2 h_2 + 2(n_3 + 1) h_1]^2}$$

$$r_{n3} = \sqrt{(x - x_0)^2 + (y - y_0)^2 + [2n_1(h_1 + h_2) + 2(n_2 + 1) h_2 + 2h_3 h_1]^2}$$

$$r_{n4} = \sqrt{(x - x_0)^2 + (y - y_0)^2 + [2(n_1 + 1)(h_1 + h_2) + 2n_2 h_2 + 2n_3 h_1]^2}.$$

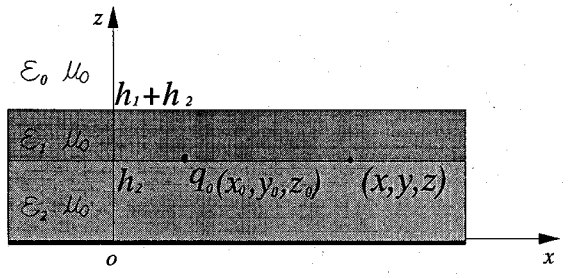


Fig. 3. Point charge in a substrate–superstrate structure.

It turns out that the rigorous solution (16) converges very slowly, especially when the source-to-field point distance is large. To check the accuracy of the complex image solution (16), we would rather calculate the inverse transformation of (13) directly by using numerical integration. Table III lists the complex image coefficients for two sets of dielectric parameters. It is seen that, analogous to the case of open microstrip substrate, the complex image coefficients in Table III are also complex conjugates of one another. Table IV lists some values of the potential function $\Phi$ computed by the complex image solution (16) and by numerical integration. It is seen that the difference is again less than 0.1% for the field-to-source point distances tabulated.

For the case of arbitrary $z$ and $z_0$, one can easily derive a spectral potential function using transmission line theory [5]. Then the spatial image solution of the potential function can be obtained by following the same steps as (6) to (11).

### *D. Point Charge in a General Multilayered Medium Structure*

By a general multilayered medium structure, we mean that (i) the layered medium may have any number of layers and (ii) the source and field points may be located at any position within the layered medium. Fig. 4 shows a point charge in a general multilayered medium structure, where an exact image solution is impractical and unavailable.

For the derivation of the spectral-domain scalar potential $\tilde{\Phi}$ in a general multilayered medium, we can use the transmission line theory given in [5]. $\tilde{\Phi}$ generally has the form

$$\tilde{\Phi} = \frac{q_0}{2\epsilon_0 \epsilon_{rs} \gamma} \cdot F(\gamma, z, z_0) \tag{17}$$

where $\epsilon_{rs}$ is the relative dielectric constant of the layer in which the point charge $q_0$ is located. In general, the spatial coordinates $z$ and $z_0$ in $F(\gamma, z, z_0)$ may not appear as an exponential function as in (6). To avoid the sophisticated expression of the spatial potential function, for arbitrary $z$ and $z_0$, we would rather fix $z$ and $z_0$ in numerical computations.

Then, we first take the limit of $F(\gamma, z, z_0)$ at $\gamma \to \infty$, i.e.,

$$\lim_{\gamma \to \infty} F(\gamma, z, z_0) = F_0. \tag{18}$$

As the second step, we subtract the limit $F_0$ from the original function $F(\gamma)$ and make the following numerical match:

$$F(\gamma, z, z_0) - F_0 \doteq \sum_{i=1}^{N} a_i e^{b_i \gamma}. \tag{19}$$

Substituting (19) into (17) and taking the inverse Fourier transformation of $\tilde{\Phi}$, we get the complex image solution of $\Phi$:

$$\Phi \doteq \frac{q_0}{4\pi \epsilon_0 \epsilon_{rs}} \left( F_0 \frac{1}{r_0} + \sum_{i=1}^{N} \frac{a_i}{r_i} \right) \tag{20}$$

where

$$r_0 = \sqrt{(x-x_0)^2 + (y-y_0)^2}$$

$$r_i = \sqrt{(x-x_0)^2 + (y-y_0)^2 + b_i^2}.$$

## III. Discussions and Conclusion

In this section, we seek an insight into the complex images by taking a point source charge in the three-layered medium of Fig. 3 as an example. The formulations for this problem are given in (12)–(16).

It is very interesting to observe the behavior of the spectral function $A(\gamma)$ given by (12). Fig. 5 shows the original spectral function $A(\gamma)$ as well as the spectral function with a constant $A_0$ subtracted, in the interval $\gamma \in [0, T_0]$ where the exponential matching (14) is made. It is observed that if the three-layered media is replaced by a homogeneous medium with the effective dielectric constant of $(\epsilon_{r1} + \epsilon_{r2})/2$, there will be a spectral error. The complex images can correct the spectral error effectively.

The complex image series is obtained through Prony's method, where the number of complex images is prescribed. We varied the number of images from 2 to 5. It is found that two images can give the potential function $\Phi$ with precision up to four decimal digits, and five images give six decimal digits. In practical problems, two complex images are sufficient.

In numerical calculations, the matching truncation point $T_0$ is chosen such that when $\gamma > T_0$, the spectrum function becomes negligible. We chose $T_0 = 10.0/(h_1 + h_2)$ in this example.

The spectral function $A(\gamma)$ is a real function in the electrostatic case. The success of the complex image technique in this paper implies that a real function could be accurately approximated by a short series of complex functions.

The complex image technique is simple and quickly convergent and has been found to be very accurate, e.g., error $\sim 0.1\%$ in Tables II and IV, even for multilayered media. The reason may be that there are extra degrees of freedom in the imaginary components of the amplitudes and locations of the complex images. This is in contrast to the real amplitudes and real locations of the static images. The field from each complex image may be complex. For the electrostatic field, the imaginary portions of the

TABLE III
COMPLEX IMAGES OF A POINT CHARGE IN A SUBSTRATE–SUPERSTRATE STRUCTURE

| | $\epsilon_{r1}=9.8$, $h_1=1.0$ mm<br>$\epsilon_{r2}=2.55$, $h_2=1.0$ mm | | $\epsilon_{r1}=2.55$, $h_1=1.0$ mm<br>$\epsilon_{r2}=9.8$, $h_2=1.0$ mm | |
|---|---|---|---|---|
| $i$ | $a_i$ | $b_i$ ($\times 10$ mm) | $a_i$ | $b_i$ ($\times 10$ mm) |
| 1 | 0.9398 | −0.1716 | −0.5445 | −0.1964 |
| 2 | −1.2634 + $j$3.1439 | −0.7148 + $j$0.1461 | 0.6575E-1 + $j$0.1521E-1 | −0.4516 − $j$0.1496 |
| 3 | −1.2634 − $j$3.1439 | −0.7148 − $j$0.1461 | 0.6575E-1 − $j$0.1521E-1 | −0.4516 + $j$0.1496 |

TABLE IV
POTENTIAL FUNCTION $\Phi$ COMPUTED BY THE EXACT IMAGE SOLUTION AND THE COMPLEX IMAGE SOLUTION
$\left(z_0=0,\ z=0,\ \rho=\sqrt{(x-x_0)^2+(y-y_0)^2}\right)$

| | $\epsilon_{r1}=9.8$, $h_1=1.0$ mm<br>$\epsilon_{r2}=2.55$, $h_2=1.0$ mm | | $\epsilon_{r1}=2.55$, $h_1=1.0$ mm<br>$\epsilon_{r2}=9.8$, $h_2=1.0$ mm | |
|---|---|---|---|---|
| $\rho$ (mm) | Numerical Integration | Complex Image Solution | Numerical Integration | Complex Image Solution |
| 0.1 | 1623.00 | 1622.12 | 1521.93 | 1522.00 |
| 0.6 | 270.69 | 270.20 | 176.94 | 176.99 |
| 1.1 | 142.92 | 142.91 | 63.23 | 63.22 |
| 1.6 | 91.68 | 91.90 | 27.55 | 27.53 |
| 2.1 | 63.30 | 63.52 | 13.17 | 13.15 |
| 3.1 | 33.22 | 33.31 | 3.58 | 3.58 |

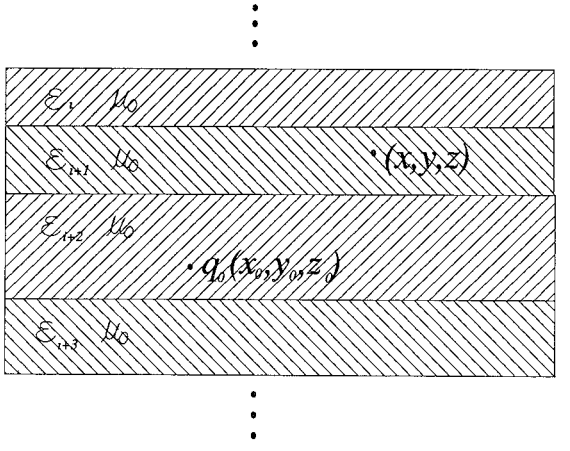


Fig. 4. Point charge in a general multilayered medium structure.

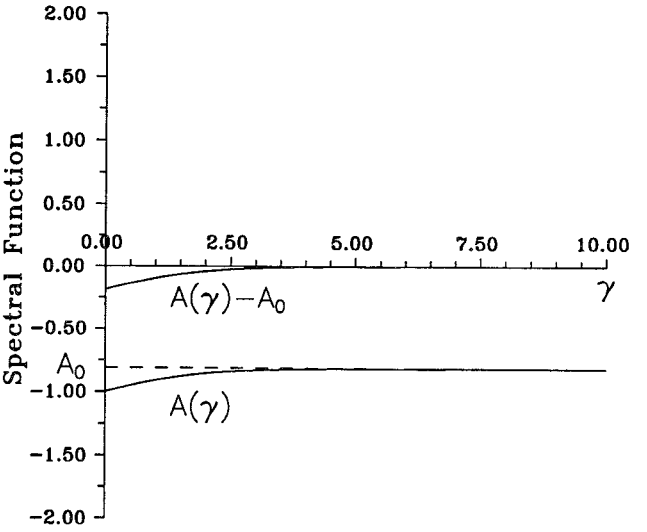


Fig. 5. Spectral function $A(\gamma)$ (see eq. (12)) for a substrate–superstrate structure.

fields cancel when the fields of the complex images are summed. This cancellation is due to the complex conjugate pairing of the images.

The complex images for the static field are discovered after those of the dynamic field [6]–[9]. However, as the static field is physically easier to understand than the dynamic field, these static complex images can be used to gain an insight into the behavior of the corresponding dynamic ones.

Recently, this complex image technique was applied to analyze multiconductor transmission lines in multilayer dielectric media [12]. With all the computations performed on a personal computer, the agreement between capacitance matrices and available data is within 1%.

This paper studies only examples of electrostatic fields. Evidently the same complex image technique can be applied to other static examples, such as those of magnetostatics. The combination of them should be useful for the multilayered medium found in digital circuits.

## ACKNOWLEDGMENT

The authors wish to thank the reviewers for pointing out some errors in the original manuscript.

## REFERENCES

[1] P. Silvester, "TEM wave properties of microstrip transmission lines," *Proc. Inst. Elec. Eng.*, vol. 115, pp. 43–48, 1968.
[2] A. Farrar and A. T. Adams, "Multilayer microstrip transmission lines," *IEEE Trans. Microwave Theory Tech.*, vol. MTT-22, pp. 889–891, 1974.

[3] G. E. Howard, "Analysis of passive and active microwave integrated circuits by field approach," M.Sc. thesis, University of Waterloo, 1988.
[4] C. Wei, R. F. Harrington, J. R. Mautz, and T. K. Sarkar, "Multiconductor transmission lines in multilayered dielectric media," *IEEE Trans. Microwave Theory Tech.*, vol. MTT-32, pp. 439–450, 1984.
[5] R. Crampagne, M. Ahmadpanah, and J. Guiraud, "A simple method for determining the Green's function for a large class of MIC lines having multilayered dielectric structures," *IEEE Trans. Microwave Theory Tech.*, vol. MTT-26, pp. 82–87, 1978.
[6] D. G. Fang, J. J. Yang, and G. Y. Delisle, "Discrete image theory for horizontal electric dipoles in a multilayered medium," *Proc. Inst. Elec. Eng.*, vol. 135, pt. H, pp. 297–303, 1988.
[7] Y. L. Chow, J. J. Yang, D. G. Fang, and G. E. Howard, "A closed-form spatial Green's function for the thick microstrip substrate," *IEEE Trans. Microwave Theory Tech.*, vol. 39, 588–592, Mar. 1991.
[8] J. J. Yang, Y. L. Chow, and D. G. Fang, "Complex images of a 3-D dipole above and within a lossy ground," *Proc. Inst. Elec. Eng.*, pt. H, to be published.
[9] J. J. Yang, Y. L. Chow, G. E. Howard, and D. G. Fang, "The effect of metallic top cover on the feedback characteristics of microstrip amplifiers," to be submitted.
[10] Y. L. Chow and C. Charalambous, "Static-field computation by the method of optimised simulated images," *Proc. Inst. Elec. Eng.*, vol. 126, pp. 123–125, 1979.
[11] R. W. Hamming, *Numerical Methods for Scientists and Engineers*. New York: Dover, 1973, pp. 620–622.
[12] J. J. Yang, G. E. Howard, and Y. L. Chow, "Complex image method for analyzing multiconductor transmission lines in multilayered dielectric media," to be presented at *1991 Int. IEEE/AP-S Symp.*, London, Ontario, June 24–28, 1991.

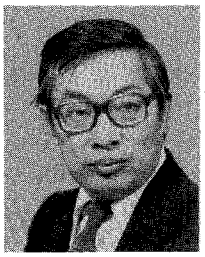

**Y. Leonard Chow** (S'60–M'65) received the B.Eng. degree in 1960 from McGill University, Montreal, Que., Canada, and the M.A.Sc. and Ph.D. degrees in 1961 and 1965 from the University of Toronto, Toronto, Ont., Canada.

From 1964 to 1966, he worked for the National Radio Astronomy Observatory, Charlottesville, VA. As a consequence, in 1974 he designed the array configuration for the Very Large Antenna Array, which comprises 27 85-ft parabolic reflectors and is located in Socorro, NM. In 1966 he joined the University of Waterloo, Waterloo, Ontario, Canada, and became a Professor in the Department of Electrical and Computer Engineering. Presently his research deals with the numerical simulation of field effects. The field effects range from high-voltage dc fields to antennas and to fields of microwave integrated circuits, both linear and nonlinear. In the microwave integrated circuit area, he is a consultant to both the Communications Research Centre, Canada, and EEsof Inc., California. He is the principal author of the field-theory-based MIC package EMSim, of EEsof Inc.

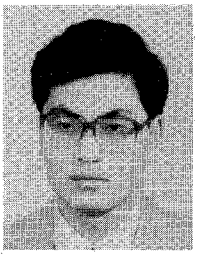

**Jian Jun Yang** (M'90) was born in Hebei Province, China, on March 30, 1966. He received the B.Eng. and M.Eng. degrees in electrical engineering from the East China Institute of Technology, Nanjing, China, in July 1984 and March 1987 respectively. In January 1989 he received the Ph.D. degree in electromagnetics from the University of Electronics Science and Technology, Chengdu, China.

From January to December of 1989, he was an Assistant Professor in the Department of Electrical Engineering, East China Institute of Technology, Nanjing, China. Since January 1990, he has been a Visiting Research Assistant Professor in the Department of Electrical and Computer Engineering, University of Waterloo, Waterloo, Ontario, Canada. His research interests include microwave integrated circuits, microstrip antennas and frequency selective surfaces, circuit board EMC, optoelectronic integrated circuits, and grounding facilities in power delivery.

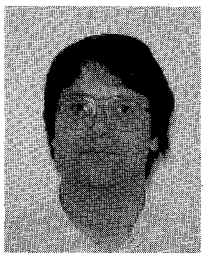

**Gregory E. Howard** was born in Ontario, Canada, on April 14, 1962. He received the BASc and MASc degrees in electrical engineering from the University of Waterloo, Waterloo, Ontario, Canada, in May 1985 and May 1988 respectively. He is currently working towards the Ph.D. degree in electrical engineering at the University of Waterloo and expects to complete his degree in the summer of 1991. His research interests include MIC's, microstrip antennas, circuit board EMC, and software engineering for electromagnetic numerical methods.